ACS Chemical Neuroscience

Research Article

pubs.acs.org/chemneuro

# Tabersonine Inhibits Amyloid Fibril Formation and Cytotoxicity of Aβ(1−42)

Tianhan Kai,[†] Lin Zhang,[†] Xiaoying Wang,[‡] Aihua Jing,[‡,§] Bingqing Zhao,[‡] Xiang Yu,[∥] Jie Zheng,*[,∥] and Feimeng Zhou*[,‡]

[†]College of Chemistry and Chemical Engineering, Central South University, Changsha, Hunan 410083, P. R. China

[‡]Department of Chemistry and Biochemistry, California State University, Los Angeles, Los Angeles, California 90032, United States

[§]College of Medical Technology and Engineering, Henan University of Science and Technology, Luoyang, Henan 471003, P. R. China

[∥]Department of Chemical and Biomolecular Engineering, The University of Akron, Akron, Ohio 44325, United States

Supporting Information

**ABSTRACT:** The misfolding and aggregation of amyloid beta (Aβ) peptides into amyloid fibrils are key events in the amyloid cascade hypothesis for the etiology of Alzheimer's disease (AD). Using thioflavin-T (ThT) fluorescence assay, atomic force microscopy, circular dichroism, size exclusion chromatography, surface plasmon resonance (SPR), and cytotoxicity tests, we demonstrate that tabersonine, an ingredient extracted from the bean of *Voacanga africana*, disrupts Aβ(1−42) aggregation and ameliorates Aβ aggregate-induced cytotoxicity. A small amount of tabersonine (e.g., 10 μM) can effectively inhibit the formation of Aβ(1−42) (e.g., 80 μM) fibrils or convert mature fibrils into largely innocuous amorphous aggregates. SPR results indicate that tabersonine binds to Aβ(1−42) oligomers in a dose-dependent way. Molecular dynamics (MD) simulations further confirm that tabersonine can bind to oligomers such as the pentamer of Aβ(1−42). Tabersonine preferentially interact with the β-sheet grooves of Aβ(1−42) containing aromatic and hydrophobic residues. The various binding sites and modes explain the diverse inhibitory effects of tabersonine on Aβ aggregation. Given that tabersonine is a natural product and a precursor for vincristine used in cancer chemotherapy, the biocompatibility and small size essential for permeating the blood−brain barrier make it a potential therapeutic drug candidate for treating AD.

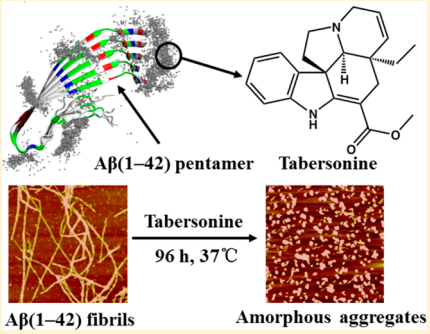


**KEYWORDS:** *Tabersonine, Aβ(1−42) fibrillation, Alzheimer's disease, cytotoxicity, aggregation, disaggregation*

Alzheimer's disease (AD) is the most prevalent form of dementia. Post-mortem analyses of AD patients have revealed that senile plaques, a hallmark of AD, contain fibrillar aggregates of amyloid-β (Aβ) peptides of 39−43 amino acids.[1−4] The amyloid cascade hypothesis[2] presumes that amyloid aggregates, self-assembled from misfolded Aβ peptides, affect the structure and functions of neuronal cells and stimulate cell apoptosis,[5−9] leading to synaptic dysfunction and neurodegeneration.

The complexity associated with amyloidogenesis has rendered challenges to studies of biochemical and physiological aspects of AD and the development of effective drugs against amyloid diseases. Current strategies to reduce Aβ production include (i) decreasing the expression of the amyloid precursor protein (APP),[10] (ii) inhibiting the activities of β and γ secretases,[11−13] and (iii) dissociating toxic Aβ aggregates.[14,15] As APP and secretases have biological functions needed by the brain, searching for aggregation inhibitors might be an approach with fewer side effects. Short peptides[16−19] (β-sheet breaker peptides) and small organic molecules[14,20−23] have been explored for their inhibitory ability. Most peptide-based inhibitors are derived from the Aβ sequence, particularly from the central hydrophobic segment, Aβ17−21 (LVFFA),[16−18] and C-terminal fragment, Aβ39−42 (VVIA).[24] These peptides as β-sheet breakers have been shown to reduce Aβ aggregation and to alleviate Aβ-induced neurotoxicity. However, the vulnerability of peptides to enzymatic degradation and poor permeability through the blood−brain barrier (BBB)[25] are limitations. Recently, low-molecular-weight and lipophilic compounds derived from recombinatory libraries or extracted from natural products have shown great promise in inhibiting Aβ aggregation.[14] Owing to their small size and high permeability through the BBB, they are attractive pharmaceutical drug candidates for treating AD. Several compounds, such as LY450139,[26] simvastatin[10] and scyllo-inostol,[20,21] are currently undergoing clinical trials. Scyllo-inostol is particularly effective in inhibiting Aβ fibril assembly, converting toxic Aβ aggregates into nontoxic β-structured micelle conformers, and protecting primary neurons from Aβ oligomer-induced toxicity. Hexadecyl-*N*-methylpiperidinium bromide, nitrophenols, and

**Received:** January 10, 2015
**Revised:** April 14, 2015
**Published:** April 15, 2015





DOI: 10.1021/acschemneuro.5b00015
*ACS Chem. Neurosci.* 2015, 6, 879−888

tricyclic pyrone have also been reported as synthetic compounds to inhibit the formation of Aβ fibrils, and curcumin, a major curcumoid in the popular South Asian spice tumeric, as a natural product to disaggregate performed Aβ fibrils.[22,27−29] However, the inhibition mechanisms of many of such compounds are not clearly understood or have not been thoroughly investigated with biophysical and biochemical methods.

Computational methods have assisted drug development by shedding light on the interactions between small molecules and Aβ oligomers. In particular, molecular dynamics (MD) simulations can provide detailed structural and energetical information at the atomic level about Aβ unfolding and aggregation and can help to determine binding affinity and sites of small molecules.[30−35] For example, morin can penetrate into the hydrophobic core of fibrils to disrupt the Asp23−Lys28 salt bridge and backbone hydrogen bonding between neighboring Aβ peptides.[36] Combining MD simulation with different biophysical and cellular assays, one of us has reported that tanshinones, ingredients from the Chinese herb Danshen (*Salvia miltiorrhiza Bunge*), preferentially bind to a hydrophobic β-sheet groove formed by the C-terminal residues I31−M35 and M35−V39 and several aromatic residues.[37] Such structurally based binding information helps to interpret the prevention of Aβ fibril formation and dissociation of preformed Aβ fibrils observed experimentally.

Herein, we report on tabersonine (cf. structure in Figure 1), an indole alkaloid extracted from the beans of *Voacanga*, as a

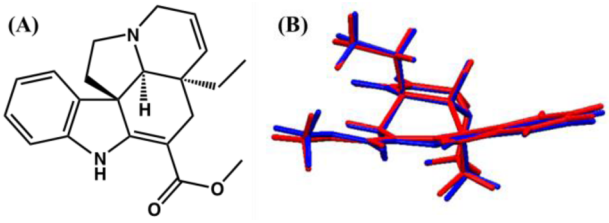


**Figure 1.** Structure of tabersonine (A). Two overlapping stick models of tabersonine (B) deduced from molecular dynamics (blue) and quantum mechanics (red).

potent inhibitor against Aβ(1−42) aggregation and toxicity. As a traditional medicine in Africa, *Voacanga* is used to treat a wide range of diseases, including leprosy, convulsions in children, and infant tonic seizures.[38] The decoction of the stem bark and root can also effectively treat mental disorders. Tabersonine itself is a type of *Catharanthus* (or *Vinca*) *herbacea* and has been widely used as the precursor of vincristine for cancer chemotherapy.[39,40] We envision that the planar portion of tabersonine and its aromatic ring structure should be able to interfere with the ordered β-sheet stacking and aggregation of Aβ(1−42) through intercalation and π−π interaction. Moreover, if tabersonine can attach to β-sheet-containing oligomers and fibrils, then the side chains and the carboxylic acid group could introduce steric hindrance and some hydrophilicity to disorganize β-sheet-containing Aβ(1−42) assemblies. Indeed, thioflavin-T (ThT) fluorescence, atomic force microscopy (AFM), circular dichroism (CD), size exclusion chromatography (SEC), surface plasmon resonance (SPR), and cell viability assays all indicate that tabersonine can effectively reduce toxic Aβ(1−42) aggregates by inhibiting the fibrillation process and changing the fibrillogenesis pathway, leading to the formation of largely innocuous amorphous aggregates. More importantly, tabersonine is capable of disassembling preformed Aβ(1−42) fibrils. MD simulations further confirm that tabersonine can strongly bind to aromatic and hydrophobic residues of the Aβ(1−42) in oligomers to disrupt the Aβ−Aβ interactions, thereby changing the overall aggregation behavior of Aβ(1−42).

## RESULTS AND DISCUSSION

**Tabersonine Inhibits Aβ(1−42) Fibril Formation and Disintegrates Preformed Fibrils.** Amyloid fibril formation or disintegration can be verified by the thioflavin-T (ThT) assay.[41,42] In Figure 2, a characteristic sigmoidal curve (black

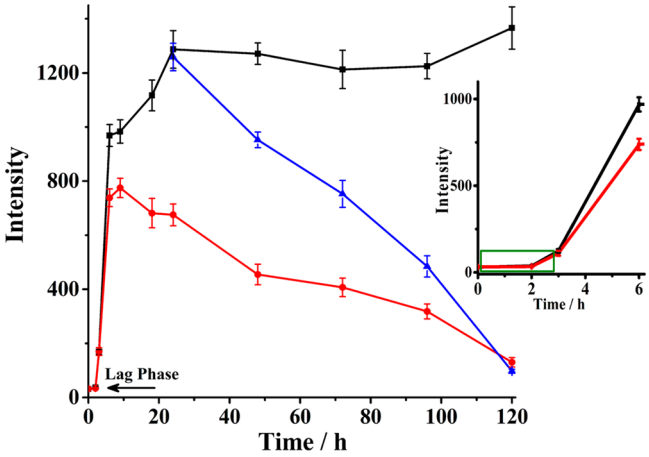


**Figure 2.** ThT fluorescence changes during incubation of 80 μM Aβ(1−42) at 37 °C in the absence (black curve) and presence of 10 μM tabersonine (red curve). The blue curve was obtained when tabersonine was added into a 80 μM Aβ(1−42) solution that had been preincubated for 24 h. Error bars are the standard deviations of three replicates. The inset is an enlarged view of the lag phase indicated.

curve) was observed for the Aβ(1−42) aggregation process, with a lag phase for ca. 3 h (inset) and a plateau appearing at ca. 24 h. The lag phase is indicative of the nucleation phase necessary for Aβ(1−42) aggregation, whereas the ThT plateau corresponds to the formation of well-ordered, β-sheet-rich Aβ(1−42) fibrils.[43] When 10 μM tabersonine was coincubated with 80 μM Aβ(1−42), the lag phase remained essentially unchanged (red curve), but no plateau (i.e., no fibrillation) appeared. Instead, the ThT fluorescence gradually decreased after ∼9 h and eventually vanished at 120 h. Moreover, the highest fluorescence signal (maximum of ca. 800) is substantially lower than the ThT plateau (∼1400) recorded from an Aβ(1−42)-only solution. The lower, yet observable, ThT signal in the presence of tabersonine indicates that a low dose of tabersonine (10 μM) cannot completely inhibit Aβ(1−42) aggregation in the early hours of the incubation. It is also possible that disruption of the smaller amounts of fibrils occurs at a later stage of the incubation. Also, tabersonine does not appear to lengthen the nucleation phase. These observations are similar to those for curcumin[44] and resveratrol.[45] In addition, it also does not enhance the ThT signal by itself. In a separate experiment, we added tabersonine into a solution containing Aβ(1−42) fibrils (produced by incubation of the monomer solution for 24 h). The fluorescence signal dropped precipitously from the plateau value (blue curve) to the same end point shown by the red curve. This result suggests that tabersonine is capable of dissociating preformed Aβ(1−42)


DOI: 10.1021/acschemneuro.5b00015
ACS Chem. Neurosci. 2015, 6, 879−888

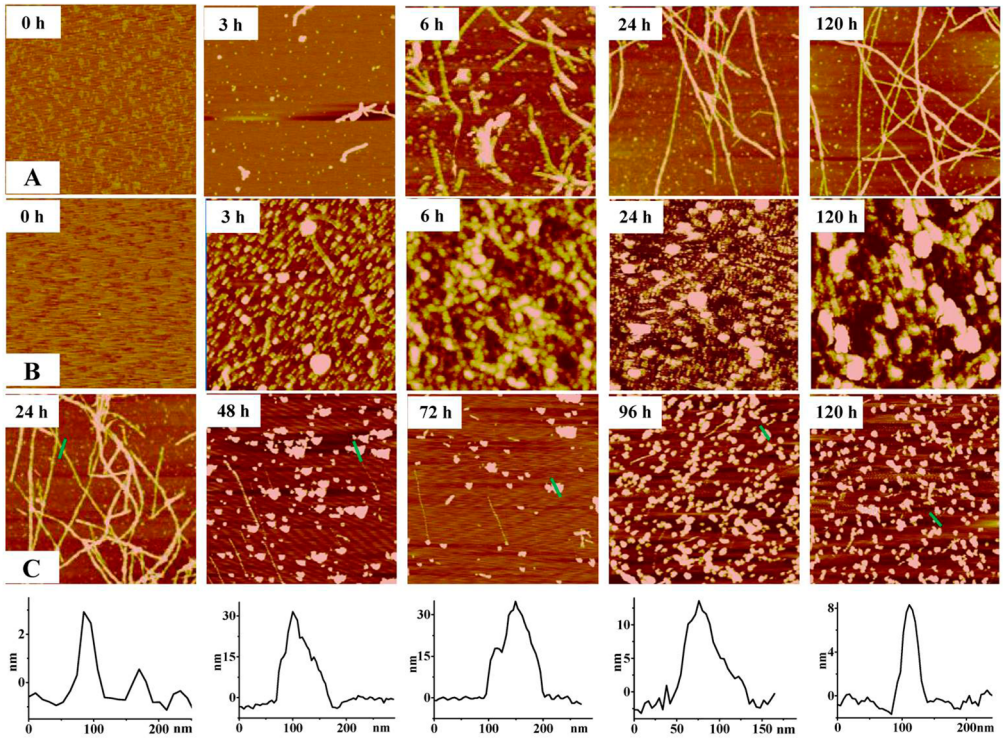


**Figure 3.** AFM images of samples taken from a 80 $\mu$M A$\beta$(1−42) solution at different incubation times (A) and a 80 $\mu$M A$\beta$(1−42) solution coincubated with 10 $\mu$M tabersonine (B). Images displayed in (C) correspond to samples from a fibril-populated solution incubated with 10 $\mu$M tabersonine for different amounts of time. The scale is 2 × 2 $\mu m^2$. The cross-sectional contours of representative aggregates denoted by green bars in (C) are also shown.

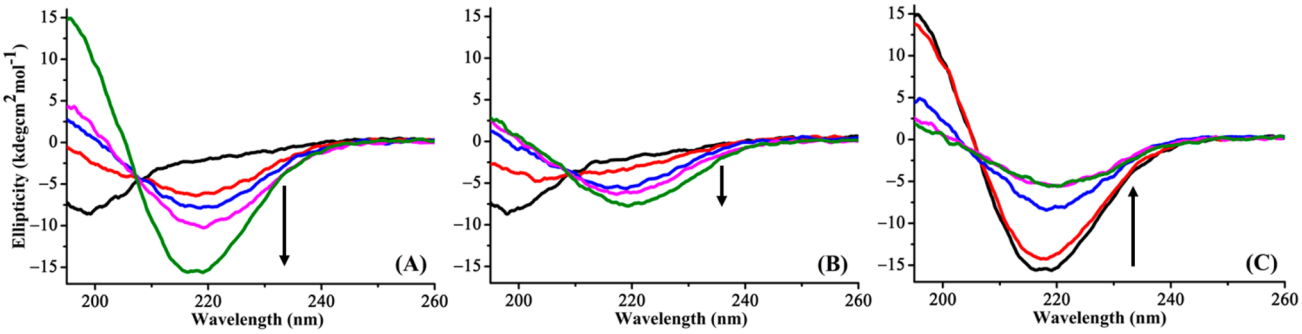


**Figure 4.** CD spectra of 80 $\mu$M A$\beta$(1−42) solutions incubated in the absence (A) and presence of tabersonine (B) for 0 (black), 3 (red), 6 (blue), 12 (magenta), and 24 h (green curve). (C) Overlay of CD spectra of solutions populated with A$\beta$(1−42) fibrils upon incubation with 10 $\mu$M tabersonine for 0 (black), 24 (red), 48 (blue), 72 (magenta), and 96 h (green curve). The arrows indicate the direction of changes in spectra with the incubation time.

fibrils. Thus, tabersonine does not affect the misfolding of A$\beta$(1−42) and the formation of metastable oligomers, and it likely binds to $\beta$-sheet structures (i.e., oligomeric nuclei and fibrils) to prevent the elongation of the nuclei/oligomers via the attachment of additional A$\beta$(1−42) monomers early in the incubation and to disrupt preformed fibrils on a longer time scale. This point is supported by the surface plasmon resonance (SPR) measurements described below.

We used AFM to identify the end products from the disaggregation of A$\beta$(1−42) fibrils by tabersonine. In the control experiment, large, globular aggregates and short protofibrils were observed in an A$\beta$(1−42) solution after 3 h of incubation (cf. images juxtaposed in row A of Figure 3), consistent with the lag phase in Figure 2. After 6 h, more protofibrils were produced, and after 24 h, mature A$\beta$(1−42) fibrils dominated. The fibrils formed at 24 and 120 h exhibit similar morphology and density, suggesting that the fibrillation process had reached equilibrium with the oligomers and monomers after 24 h. However, in the presence of tabersonine, the morphology of the A$\beta$(1−42) aggregates (Figure 3, row B) was dramatically different from those shown in row A. After 3 h, A$\beta$(1−42) aggregates with heights exceeding 20 nm are substantially larger, denser, and more irregular. As the incubation progresses, these irregular aggregates appear to have agglomerated into bulky amorphous aggregates with sizes ranging from 50 to 200 nm (cf. images taken after 3 h). After 120 h, amorphous aggregates became predominate. Recall that in Figure 2 the ThT fluorescence decreased after 6 h in the presence of tabersonine. This observation suggests that the relatively large oligomers have incorporated tabersonine molecules, preventing A$\beta$(1−42) oligomers from further growing into mature fibrils. That more than 90% of the


DOI: 10.1021/acschemneuro.5b00015
ACS Chem. Neurosci. 2015, 6, 879−888

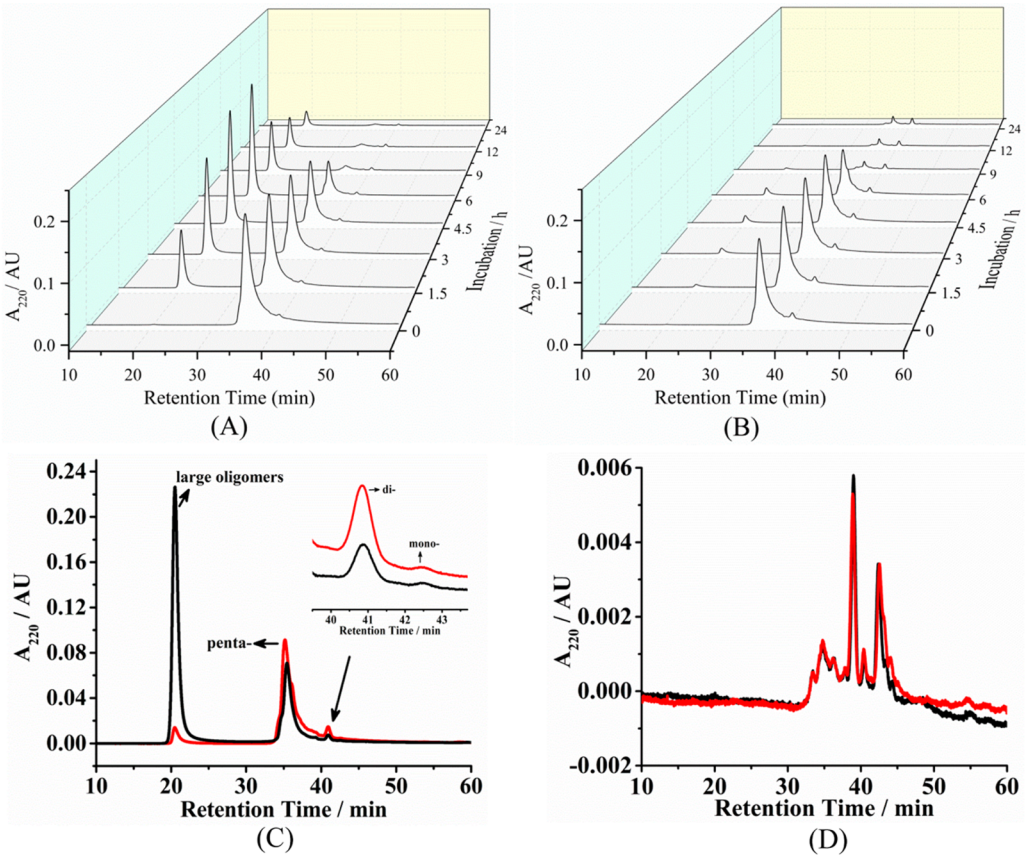


**Figure 5.** Size exclusion chromatograms of (A) 80 $\mu$M A$\beta$(1−42) incubated for different times at 37 °C. (B) Same as (A) but with 10 $\mu$M tabersonine present at the beginning of the incubation. (C) Chromatogram of a 80 $\mu$M A$\beta$(1−42) solution incubated alone for 6 h (black) overlaid with that coincubated with 10 $\mu$M tabersonine (red), with the putative monomer, dimer, pentamer, and large soluble oligomers identified. The inset shows that the A$\beta$(1−42) monomer and dimer have retention times of 42.42 and 40.78 min, respectively. (D) Overlaid chromatograms of a solution containing 10 $\mu$M tabersonine coincubated with preformed fibrils for 24 (black) and 96 h (red).

induced ThT fluorescence was annihilated at 120 h in Figure 2 suggests that the amorphous aggregates have rather disordered structures.

Formation of A$\beta$(1−42) fibrils after 24 h of incubation was confirmed by the leftmost image in row C of Figure 3. Interestingly, after incubating these A$\beta$(1−42) fibrils with 10 $\mu$M tabersonine for 24 h, the preformed fibrils were either significantly truncated into shorter and thinner fibrils or completely disintegrated into amorphous aggregates. The effect is more pronounced after 48 h, as evidenced by the formation of irregular, amorphous aggregates. After 120 h, fibrils were replaced by amorphous aggregates. Morphological changes can be visualized from the cross-sectional contours of the representative aggregates. It is worth mentioning that the AFM tip diameter we used (∼20 nm) is larger than the width of A$\beta$(1−42) fibrils. As a result, the width of A$\beta$(1−42) fibrils appears to be larger than the actual size (10 nm) due to the tip-broadening effect.[46] The aggregates shown in row C have similar morphologies to those in row B, although the sizes are generally smaller.

Next, we employed circular dichroism (CD) spectroscopy to monitor conformational changes in A$\beta$(1−42) solution incubated without (Figure 4A) and with tabersonine (Figure 4B). In both solutions, at the beginning of the incubation, the natively unstructured conformation of A$\beta$(1−42), signified by the peak at 197 nm, was observed. This peak disappeared after 3 h, and the peak at 217 nm, which corresponds to $\beta$-sheets, appeared. The continuous increase in the peak height indicates that as the incubation prolongs, $\beta$-sheet-rich oligomers and fibrils are produced. This is consistent with our AFM results. In the presence of tabersonine, this peak is much attenuated (less than 50% of those in Figure 4A), suggesting that less fibrils are produced, again in agreement with our AFM observation. To ensure that the decrease in the CD signal is not due to the precipitation of amorphous aggregates, we shook vigorously or sonicated the solution in the cuvette but did not find any change in the resultant spectra. Because our AFM imaging revealed that the effect of tabersonine is to divert the A$\beta$(1−42) fibrillation pathway to the formation of or disrupt existing fibrils into amorphous aggregates, the existence of the 217 nm peak after 24 h incubation (green curve in Figure 4B) implies that amorphous aggregates also contain some $\beta$-sheets. In our previous studies on $Cu^{2+}$-accelerated A$\beta$(1−42) aggregation,[47] we posited that, unlike fibrils produced from ordered stacking of oligomers, amorphous aggregates are formed from random agglomeration of A$\beta$(1−42) oligomers and monomers. Owing to the disordered intermingling of oligomers and monomers, less monomers are converted into oligomers or fibrils, and the amount of $\beta$-sheets present in the A$\beta$(1−42) solution coincubated with tabersonine is therefore smaller. When preformed fibrils were incubated with tabersonine (Figure 4C), they were disintegrated into amorphous aggregates of various sizes. It is also likely that in both cases the smaller aggregates dislodged from fibrils have their $\beta$-sheets disrupted


DOI: 10.1021/acschemneuro.5b00015
ACS Chem. Neurosci. 2015, 6, 879−888

due to the interaction between A$\beta$(1−42) oligomers/fibrils and tabersonine (vide infra).

Size exclusion chromatography (SEC) has been used to separate A$\beta$ monomers from soluble oligomers formed under different experimental conditions.[48−51] We resorted to SEC to correlate the species that might be targeted by tabersonine at different incubation times. Assignments of the peaks to different oligomeric species, as shown in Figure 5C, were made by using a calibration curve (Figure S2). The A$\beta$(1−42) chromatogram at 0 h incubation (Figure 5A) has all of the essential features and relative positions reported by Smith and co-workers.[49] Note that a typical chromatographic experiment (including sample injection and separation) requires about 50−60 min. During this period, A$\beta$(1−42) monomers (retention time $t_R$ = 42.42 min) have largely oligomerized into pentamers and possibly hexamers (retention time $t_R$ = 35.45 min). The inability to clearly resolve pentamers from hexamers[49] is the result of the influence of a variety of factors, such as hydration and dependence (or lack of) of shape on the size of the aggregates, on the elution time. The putative pentamer/hexamer peak decreased with incubation time, whereas the large soluble oligomers ($t_R$ = 20.50 min, with an overall molecular weight greater than 300 kDa) increased in the first 6 h and then decreased thereafter. This is in contrast to Figure 5B, which was recorded from A$\beta$(1−42) solutions coincubated with tabersonine. The putative pentamer/hexamer peak is lower at 0 h, which can be rationalized by the formation of some insoluble aggregates due to the interaction between tabersonine and A$\beta$(1−42) pentamer (Figure 5A, 0 h or, more accurately, detected 50−60 min after fresh preparation of the solution).[50,52] Notice that these insoluble aggregates, which are not separable by SEC, were not observed by AFM. This inconsistency can be explained by the difference between AFM sample preparation and SEC separation. For AFM sample preparation, the freshly prepared mixture of A$\beta$(1−42) and tabersonine was cast onto the mica sheet, and the solution was dried under $N_2$ in a few minutes (instead of 50−60 min). In such a short time frame, few insoluble aggregates were produced. Also noteworthy is that the peak corresponding to the large, soluble oligomers is substantially smaller. Such a phenomenon has also been noted by us[51] and others.[50] The significant reduction in the amount of oligomers is due to their conversion into amorphous aggregates. Such a conversion decreases the number of $\beta$-sheets in solution, which explains why the CD peaks in Figure 4B are much smaller. The nearly complete disappearance of the oligomer peaks after 9 h of incubation is consistent with the AFM findings on the formation of large, insoluble aggregates (cf. Figure 3). We also carried out an SEC separation of soluble A$\beta$(1−42) species disintegrated from preformed A$\beta$(1−42) fibrils by tabersonine. After 24 h incubation, few A$\beta$(1−42) soluble oligomers and monomers existed in solution (cf. black curve in Figure 5D; note that the scale is 40 times smaller than those of Figure 5A−C). Extension of the coincubation time to 96 h (red curve) did not increase the monomer and oligomer concentrations. Taken together with our AFM results (vide supra), it is evident that tabersonine dissociates A$\beta$(1−42) fibrils into insoluble amorphous aggregates.

We conducted SPR measurements to verify that tabersonine binds directly to A$\beta$(1−42) monomers and oligomers (Figure S3A,B). When freshly prepared A$\beta$(1−42) samples were injected, the sensor surface was largely covered with monomers, with a small amount of oligomers readily formed in solution immobilized. On the other hand, incubated samples produced sensors covered with oligomers of different sizes and a small number of monomers. Both types of surfaces were found to be stable, suggesting that the immobilized A$\beta$(1−42) molecules are covalently linked and do not undergo further aggregation. Tabersonine was found not to adsorb onto sensors without A$\beta$(1−42) immobilized. Owing to the surface inhomogeneity, our kinetic analysis under the assumption of 1:1 binding stoichiometry yields only the apparent dissociation constant, $K_D'$. Moreover, the approximately linear dose−response curve over a range of tabersonine concentrations (Figure S3C) suggests that the binding stoichiometry could vary with the tabersonine concentration.[53] The stoichiometry was determined by

$$S = (R_{eq}/R_L)(MW_L/MW_A)$$

where $S$ is the number of tabersonine molecules bound per immobilized A$\beta$(1−42) oligomer. $R_L$ is the number of immobilized A$\beta$(1−42) oligomers, and $MW_L$ and $MW_A$ are the molecular weights of pentamer and tabersonine, respectively. We chose the pentamer because it is the predominant oligomeric species under the experimental conditions (cf. Figure 5). The increase in stoichiometry from 0.2:1 to 1.3:1 between 12.5 and 200 $\mu$M tabersonine implies that tabersonine interacts with multiple binding sites on the A$\beta$(1−42) oligomers, instead of binding to a single pocket.[53] Despite the complexity encountered in our SPR analysis, the $K_D'$ value corresponding to A$\beta$(1−42) oligomers, 69 ± 7 $\mu$M, is almost an order of magnitude smaller than that to the monomer, 535 ± 66 $\mu$M. Thus, tabersonine binds to A$\beta$(1−42) oligomers more strongly than to A$\beta$(1−42) monomers.

**Tabersonine Reduces A$\beta$(1−42)-Inflicted Cytotoxicity.** To investigate whether the amorphous aggregates are innocuous, SH-SY5Y human neuroblasoma cells were used for cell viability assays (Figure 6). In this experiment,

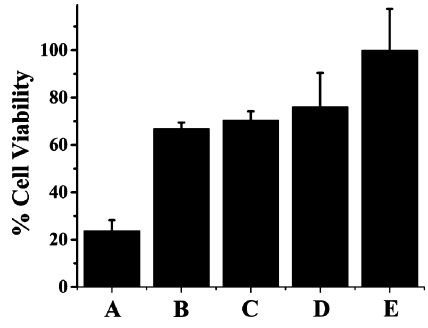


**Figure 6.** SH-SY5Y cell viability after being exposed to (A) A$\beta$(1−42) oligomers and fibrils formed by incubating 80 $\mu$M monomer solution for 24 h, (B) an A$\beta$(1−42) solution incubated with 10 $\mu$M tabersonine for 24 h, (C) a mixture of A$\beta$(1−42) fibrils and oligomers that was treated with 10 $\mu$M tabersonine for 96 h, (D) a 10 $\mu$M tabersonine-only solution, and (E) a 5 $\mu$M tabersonine-only solution. All incubations were carried out at 37 °C. The error bars are standard deviations of three different replicates collected on different days.

absorbance of the cell media containing SH-SY5Y cells was measured, and the value is regarded as 100% of cells being viable. A$\beta$(1−42) was allowed to oligomerize and fibrillize for 24 h in cell culture media, and the resultant solution was added to wells containing SH-SY5Y cells (bar A). The cell viability decreased to 24 ± 4% of the control, indicating that A$\beta$(1−42) oligomers and fibrils are cytotoxic. However, when A$\beta$(1−42)


DOI: 10.1021/acschemneuro.5b00015
ACS Chem. Neurosci. 2015, 6, 879−888

was coincubated with tabersonine for 24 h, the cell viability was rescued to 67 ± 3% (bar B). As shown by the AFM images in Figure 3B, after 24 h coincubation with tabersonine, the predominate aggregate in solution is amorphous in nature. Thus, amorphous aggregates are not cytotoxic, in line with the findings on amorphous aggregates produced under other experiments by us[37,51] and others.[45] Similar cell viability (70 ± 4%) was obtained when tabersonine was introduced to a largely A$\beta$(1−42) fibril solution for 96 h (bar C). A relatively small toxicity was found to be contributed by tabersonine at 10 $\mu$M (tabersonine alone, shown as bar D, is 76 ± 14%). Tabersonine is a precursor of vincristine whose side effects have been noted in cancer chemotherapy.[54] However, the side effects are associated with the high dosage typically required for cancer therapy (12.5−50 $\mu$g drug/kg body mass/week).[39] *In vivo* A$\beta$ peptides are present at nanomolar concentrations, which is significantly less than micromolar concentrations used for *in vitro* aggregate formation. The actual amount of tabersonine, if administered as an AD modality, would be considerably less. Indeed, we found that by decreasing the concentration to only 5 $\mu$M the toxicity was completely abolished (bar E).

**Binding Modes of Tabersonine to the A$\beta$(1−42) Pentamer.** To gain a better understanding regarding the inhibition mechanism, we performed all-atom MD simulations to study the binding modes of tabersonine to the A$\beta$(1−42) pentamer. We chose the pentamer because (1) together with hexamer it is the most abundant soluble oligomer, and its toxicity is one of the highest,[49,55,56] (2) a number of computational studies have demonstrated that the A$\beta$(1−42) pentamer with a U-bend conformation exhibits high structural stability and serves as a basic template nucleus for amyloid growth via either monomer attachment for elongation or lateral stacking,[57−59] and (3) tabersonine binds to oligomers more strongly than to monomer, as revealed by our SPR measurements. Residues 1−17 of A$\beta$(1−42) are disordered, and residues 18−26 ($\beta$-strand 1) and residues 31−42 ($\beta$-strand 2) form two antiparallel $\beta$-strands connected by a U-bend that spans across residues 27−30.[60] Residues F19 and A21 in $\beta$-strand 1 participate in hydrophobic interaction with residues G38 and V36 of $\beta$-strand 2 on its two neighboring A$\beta$(1−42) peptides. An intermolecular salt bridge between D23 and K28 stabilizes the U-bend conformation. Figure 7 shows the distribution of tabersonine molecules bound to a single A$\beta$(1−42) pentamer. In this model, accumulative positions of tabersonines were sampled by 4 ps snapshots from two independent MD trajectories. It is clearly seen that tabersonine does not disturb the structural integrity of the A$\beta$(1−42) pentamer within 30 ns. Independent of the initial positions and orientations of tabersonine molecules, tabersonine preferentially binds to the external side of both N- and C-terminal $\beta$-sheets and the U-bend. These results suggest that tabersonine does not inhibit the formation of small oligomers (e.g., pentamer or hexamer); instead, the attachment of tabersonine to the $\beta$-sheets of small oligomers hinders the elongation and lateral association of small A$\beta$(1−42) oligomers/monomers required for further growth into larger oligomers and fibrils. These results are also consistent with our findings that tabersonine does not impede oligomerization during the nucleation phase (Figure 2). Finally, the absence of any disturbance of the pentamer $\beta$-sheet structure by tabersonine in MD simulations is likely due to the short time scale of ∼30 ns because the structural disruption of A$\beta$(1−42) oligomers and fibrils by tabersonine occurs on a much longer time scale, as shown by ThT and SEC assays. Another unexplored scenario by simulation is that binding of tabersonine to A$\beta$(1−42) would interfere with the formation of the U-bend $\beta$-sheet conformation of A$\beta$(1−42). In either scenario, the capability of tabersonine to interact with oligomers and disrupt preformed fibrils is unambiguously verified by our SPR experiments (Figure S3), CD data (Figure 4B,C), and AFM images (Figure 3B,C).

To further identify the possible binding sites on the A$\beta$(1−42) pentamer, we clustered the A$\beta$(1−42)−tabersonine complex into different structural groups using a root-mean-square deviation of 5 Å as a cutoff value. Figure 8 shows the representative structures of the top six clusters, which correspond to highly populated binding sites at Asp1−His6 (Region 1), Tyr10−Val12 (Region 2), Val18−Glu22 (Region 3), Ser26−Gly29 (Region 4), Ala30−Gly37 (Region 5), and Val39−Ala41 (Region 6). Specifically, aromatic residues F4, F6, Y10, F19, and F20 along the groove of the N-terminal $\beta$-sheets in Regions 1−3 provide more favorable sites for interaction with tabersonine. The $\pi$−$\pi$ stacking between these aromatic

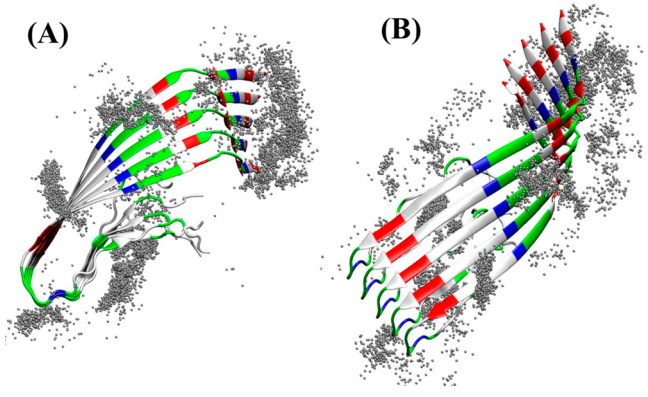


**Figure 7.** Distribution of tabersonine molecules bound to an A$\beta$(1−42) pentamer in (A) top and (B) side views. Tabersonine molecules within 5 Å from the pentamer are shown as gray spheres.

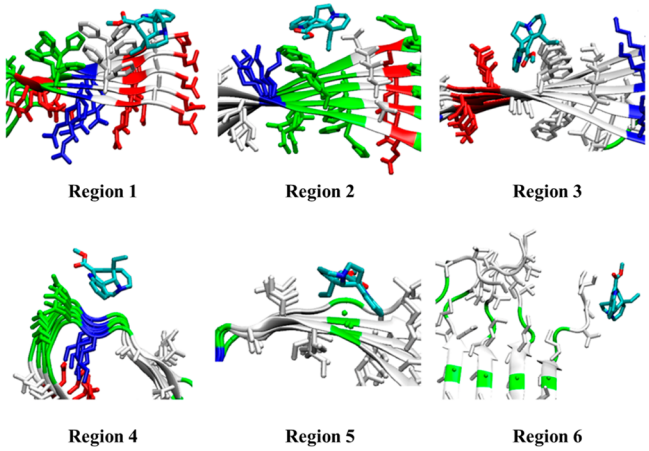


**Figure 8.** Regions of A$\beta$(1−42) with high tabersonine binding probabilities (percentages of the total population shown in parentheses): Asp1−His6 (Region 1, 16.34%), Tyr10−Val12 (Region 2, 14.24%), Val18−Glu22 (Region 3, 11.2%), Ser26−Gly29 (Region 4, 7.6%), Ala30−Gly37 (Region 5, 5.1%), and Val39−Ala41 (Region 6, 3.7%).


DOI: 10.1021/acschemneuro.5b00015
*ACS Chem. Neurosci.* 2015, 6, 879−888

residues and tabersonine would interfere with the ordered stacking of $\beta$-sheets for producing large A$\beta$(1−42) oligomers and fibrils (consistent with our CD spectra and SEC data). The binding of tabersonine to Region 1 disrupts intermolecular cross-linking between F4 and M35, whereas binding with Region 3 (Val18−Glu22) limits the hydrophobic interaction of tabersonine with F19/G38. Many studies have shown that both $\pi-\pi$ stacking and hydrophobic interaction are crucial to amyloid formation.[37,45,61,62] In Region 4, tabersonine binds to the U-bend to disrupt the D23−K28 salt bridge, which is important for stabilizing the $\beta$-sheets and stacked $\beta$-sheets. In Regions 5 and 6, tabersonine binds weakly to the C-terminal groove of the hydrophobic A21−V36 region with a random conformation, and such a hydrophobic interaction could result in the disturbance of local secondary structures of A$\beta$(1−42). Taken together, the multiple binding sites and binding modes lead to different routes to inhibit amyloid formation and to dissociate preformed fibrils.

## CONCLUSIONS

In summary, the combination of a wide range of biophysical and bioanalytical assays with computational simulation affords a detailed characterization of the tabersonine−A$\beta$(1−42) interaction. The ThT assay and AFM results demonstrate that tabersonine binds to both oligomers and fibrils, introduces disorder into the $\beta$-sheet stacking process, and disrupts preformed fibrils. The amorphous aggregates in the presence of tabersonine contain less $\beta$-sheet structures, as shown by the CD spectra. SEC data suggest that the pentamer is the predominant species during the early stages of aggregation and that large insoluble aggregates of A$\beta$(1−42) are produced when coincubated with tabersonine. SPR measurements confirmed that tabersonine has a stronger binding affinity to A$\beta$(1−42) oligomers with respect to that for the monomer. Lastly, MD simulations support our biophysical measurements and provide insight into the tabersonine−A$\beta$(1−42) interaction at the molecular level. The different A$\beta$(1−42)−tabersonine interaction modes also help to disintegrate preformed fibrils into amorphous aggregates. The small size and lipophilicity of tabersonine should facilitate its ability to cross the blood−brain barrier. In addition, as a natural product and a precursor for the cancer drug vincristine, it imposes rather low toxicity to cells. Although much more *in vivo* research is needed to validate it as a useful and clinically viable drug, our work demonstrates that the combination of molecular dynamics simulation with various biophysical methods is a powerful approach for the initial screening of drug candidates for AD or other amyloid diseases. With tabersonine identified as a potent aggregation inhibitor, the pool of potential therapeutic AD drug candidates from natural products is further expanded.

## METHODS

**Materials.** Hexafluoroisopropanol (HFIP), dipotassium phosphate, potassium phosphate monobasic, sodium hydroxide, thioflavin T (ThT), and other chemicals were purchased from Sigma-Aldrich (Milwaukee, WI). A$\beta$(1−42) was obtained from American Peptide Co. Inc. (Sunnyvale, CA). *Voacanga africana* beans were acquired from San He Tian Biological Technology Co., Inc. (Chengdu, China). All solutions were prepared with deionized water (18.2 MΩ cm$^{-1}$) collected from a water purification system (Simplicity 185, Millipore Corp, Billerica, MA). SH-SY5Y cells (human neuroblastoma) were supplied by American Type Culture Collection Inc. (Manassas, VA). Dulbecco's modified Eagle's medium (DMEM), Ham's F12 medium, fetal bovine serum (FBS), and mixtures of penicillin and streptomycin for cell cultures and cytotoxicity studies were acquired from Thermo Scientific HyClone (Logan, UT).

**Isolation of Tabersonine.** *Voacanga africana* beans (100 g) were ground and crushed into powders, which were added into 300 mL of 95% ethanol and soaked at 65 °C for 1 h. The resultant solution was filtered to yield a ∼1.2 L extract. The extract was subsequently concentrated to 50 mL and mixed with 250 mL of 1% hydrochloric acid. Upon standing for 24 h, the mixture was filtered again and purified via column chromatography using a column packed with AB-8 macroporous resin (Shanghai Hualing Resin Co., China). Elution was performed using an ethanol/water (v/v = 70:30) eluent at 0.8 mL/min. The crude tabersonine was obtained by drying the solvent on a rotary evaporator. After recrystallization with hydrochloric acid (pH 2.0) at 80 °C, tabersonine hydrochloride was obtained at 1.5 wt %. As shown in Figure S1, HPLC separation on a Kinetex C18 column (1.7 $\mu$m, 2.1 mm × 50 mm, 100 Å; Phenomenex, Torrance, CA) was conducted, and elution of tabersonine was monitored with a UV−vis detector. Gradient elution was performed with water/0.1% formic acid as eluent A and acetonitrile/0.1% formic acid as eluent B. The flow rate was 0.5 mL/min, with eluent B ramped from 25 to 100% in 10 min. High-resolution mass spectrometry (Thermo Fisher Scientific, San Jose, CA) was also used to characterize the purified product (inset of Figure S1 and Table S1). The molecular weight measured is in agreement with the reported value.[63] The chromatogram and mass spectrum are also consistent with those that we measured using a commercially available standard (Yingjie Huana Co., China).

**Solution Preparation.** The stock solution of A$\beta$(1−42) was prepared as follows. Lyophilized A$\beta$(1−42) was dissolved in 1 mg/mL HFIP and kept at room temperature for 2 h. This was followed by sonication for 30 min and then centrifugation at 14 000 rpm upon incubation at 4 °C for 30 min. The supernatant was pipetted out and freeze-dried. The as-treated A$\beta$(1−42) sample was then dissolved in 20 mM NaOH and sonicated for 1 min, which was followed by centrifugation at 14 000 rpm for 30 min. The supernatant was again pipetted out and used as the stock solution of A$\beta$(1−42). A$\beta$(1−42) concentrations were determined by UV−vis spectrophotometry with an extinction coefficient of 1410 M$^{-1}$ cm$^{-1}$ at 276 nm. Tabersonine was dissolved in water to afford a 0.2 mM stock.

**ThT Assays.** A$\beta$(1−42) solutions (80 $\mu$M) containing 100 mM phosphate buffer and 100 mM NaCl (pH 7.4) were incubated with or without 10 $\mu$M tabersonine at 37 °C. For each assay, an 7.8 $\mu$L aliquot was taken from 300 $\mu$L of either A$\beta$(1−42) or an A$\beta$(1−42)−tabersonine mixture and mixed with 92.2 $\mu$L of 20 $\mu$M ThT-containing phosphate buffer (100 mM, pH 7.4). ThT fluorescence was recorded at 490 nm, with an excitation wavelength of 450 nm, using a Hitachi F-4600 spectrofluorometer (Hitachi, Japan). The widths of the entrance and exit slits were both 10 nm.

**Atomic Force Microscopy.** Morphologies of A$\beta$(1−42) aggregates were characterized in tapping mode on a Nanoman VS atomic force microscope (Bruker, Germany) using a probe with a ∼20 nm tip diameter (MPP-11100-10, Bruker, Germany). Prior to imaging, aliquots taken from incubated A$\beta$(1−42) solutions or A$\beta$(1−42)−tabersonine mixtures were cast onto $Ni^{2+}$-treated mica sheets.

**Circular Dichroism Spectroscopy.** CD measurements were conducted on a J-810 spectropolarimeter (JASCO Inc., Tokyo, Japan) at room temperature in a 1 mm path length quartz cuvette. The spectra were collected within 195−260 at 0.1 nm intervals with a 1 nm bandwidth and a scan rate of 100 nm/min. Before each measurement, the cuvette was thoroughly shaken or sonicated for 30 s. Each spectrum is the average of three scans.

**Size Exclusion Chromatography.** Size exclusion chromatography was performed on an HPLC system (Shimudzu, Tokyo, Japan). Two columns (Yarra 3 $\mu$m SEC-2000, Phenomenex Inc., Torrance, CA) were connected in series, and the calibration curve (Figure S2, Supporting Information) was obtained using the following eight standards: human secretory IgA (385 kDa), bovine serum albumin (66 kDa), ovalbumin (45 kDa), chymotrypsinogen A (25 kDa), soybean trypsin inhibitor (20 kDa), $\alpha$-lactalbumin (14.2 kDa), aprotinin (6.5 kDa), and vitamin B12 (1.35 kDa). Elution of A$\beta$(1−42) monomers and oligomers was monitored at 220 nm. Phosphate buffer was utilized


DOI: 10.1021/acschemneuro.5b00015
ACS Chem. Neurosci. 2015, 6, 879−888

as the mobile phase, and the flow rate was 0.2 mL/min. Under the experimental conditions, A$\beta$(1−42) oligomers with molecular weights greater than 300 kDa appeared as a single peak. For each assay, a 20 $\mu$L aliquot taken from a 400 $\mu$L solution incubated in a 37 °C water bath was injected into the columns.

**Surface Plasmon Resonance (SPR).** Affinity constants of binding between tabersonine and A$\beta$(1−42) monomer/oligomers were obtained using a BI-SPR 4000 instrument (Biosensing Instrument Inc., Tempe, AZ) equipped with a two-channel flow cell on a BI dextran chip (Biosensing Instrument Inc.). 100 mM phosphate buffer (pH 7.4) containing 100 mM NaCl was employed as the running buffer and also for sample preparation. To activate the carboxylic groups on the dextran chip, a solution containing 0.4 M EDC and 0.1 M NHS was allowed to flow over the chip at 20 $\mu$L/min for 10 min. After 50 $\mu$M A$\beta$(1−42) monomer/oligomers was immobilized onto one fluidic channel at 10 $\mu$L/min for 20 min, the unreacted sites were blocked using 1.0 M ethanolamine (pH 8.0). The A$\beta$(1−42) monomer/oligomers immobilized on the dextran surface yielded ∼2170 and ∼2730 response units (RUs), respectively. The other fluidic channel was not immobilized with A$\beta$(1−42) and used as a control. Different concentrations (200, 100, 50, 25, and 12.5 $\mu$M) of tabersonine were injected at a flow rate of 120 $\mu$L/min for 2.5 min. A$\beta$(1−42) oligomers was obtained by incubating a fresh A$\beta$(1−42) solution at 37 °C for 3 h. Affinity constants were obtained from double-reference-subtracted sensorgrams fitted with the Langmuir isotherm model.

**Cell Cytotoxicity Assay.** To culture the SH-SY5Y cells, medium composed of DMEM (5mM L-glutamine), Ham's F12, FBS, and penicillin and streptomycin (v/v/v/v = 44.5:44.5:10:1) was used. The cultured cells were then transferred to a sterile 96-well plate with approximately $1 \times 10^4$ cells/well. Cells acclimatized overnight in the media in a humidified incubator under 5% $CO_2$ at 37 °C. A$\beta$(1−42) solutions and A$\beta$(1−42)−tabersonine mixtures were preincubated at 37 °C for different times, and the resultant solutions were mixed with the SH-SY5Y cells for 24 h. The viability of the SH-SY5Y cells exposed to each solution was determined with the 3[4,5-dimethylthiazol-2-yl]-2,5-diphenyl-tetrazolium bromide (MTT; EMD Inc., Gibbstown, NJ) assay. Cell viability was estimated by dividing the absorbance of wells containing samples by that of wells containing only cell culture media.

**Molecular Model.** A model based on the A$\beta$(1−42) pentamer was used to probe the tabersonine binding sites and modes. To construct an A$\beta$(1−42) pentamer, the initial monomer coordinates of an A$\beta$(17−42) peptide were taken and averaged from NMR structures (PDB code 2BEG).[37] Since the crystal structure of residues 1−16 is not available, the N-terminus was constructed and reassembled to A$\beta$(17−42), yielding a full-length A$\beta$(1−42) monomer with the $\beta$-hairpin structure. The $\beta$-hairpin A$\beta$(1−42) monomer consists of two antiparallel $\beta$-strands (residues V1−S26 and I31−A42) connected by a U-bend (residues N27−A30). Among the various structural models for A$\beta$ oligomers reported in the literature,[64,65] we used the A$\beta$(1−42) monomer with a $\beta$-strand−turn−$\beta$-strand motif as the building block to construct the A$\beta$(1−42) pentamer by stacking A$\beta$(1−42) monomers on top of each other in a parallel and registered form. The structure has an initial peptide−peptide separation of ∼4.7 Å, consistent with experimental data.[66,67] The N- and C-terminus of each A$\beta$(1−42) peptide are blocked by $COO^-$ and $NH_3^+$ groups, respectively, yielding a total net charge of −15. Five tabersonine molecules were initially and randomly placed around the A$\beta$(1−42) pentamer with a minimal distance of 10 Å to allow tabersonine to land on optimal binding sites. The A$\beta$(1−42)−tabersonine system was then solvated in a rectangular TIP3P water box. $Na^+$ and $Cl^-$ ions (total ionic strength of ∼100 mM) were added to achieve an electrically neural environment. Each system contains the A$\beta$(1−42) pentamer, five tabersonine molecules, 9000 water molecules, and 65 ions in a 107 × 57 × 60 $Å^3$ simulation box. The ParamChem tool (https://www.paramchem.org), which is compatible with the CHARMM general force field, was used to develop parameters for tabersonine. After geometry optimization at the MP2/6-31G* level by Gaussian95, the partial charges were derived by fitting the gas-phase electrostatic potential using the restrained electrostatic potential (RESP) method. To validate the force field parameters of tabersonine, a short 2 ns TIP3P water model was constructed at 310 K. The bond lengths, bond angles, and torsion angles were well-maintained in the MD simulations as compared to the quantum mechanical structure.

**Molecular Dynamics (MD) Simulation.** Simulations of the A$\beta$(1−42) pentamer−tabersonine system containing water molecules and counterions were performed using the NAMD program[68] with the CHARMM22 force field.[69] The simulation was first subject to 5000 steps of the steepest descent minimization with position constraints on A$\beta$(1−42) and tabersonine, followed by an additional 5000 steps of conjugate gradient minimization without any position constraints. After energy minimization, the system was gradually heated from 50 to 310 K in 100 ps and equilibrated at 310 K for 500 ps to adjust the size and density, with the number of atoms, pressure, and temperature kept constant. Then, 30 ns production MD runs were conducted to examine the mutual dynamics and binding events between A$\beta$(1−42) and tabersonine. Short-range van der Waals interactions were calculated by a switch function with a twin cutoff at 10 and 12 Å, whereas long-range electrostatic interactions were calculated by the particle-mesh Ewald method with a grid size of 1 Å and a real-space cutoff of 14 Å. The RATTLE algorithm was applied to constrain all covalent bonds involving hydrogen atoms, so a time step of 2 fs was used in velocity verlet integration. Each system was run twice for validation with the different starting coordinates and velocities. MD trajectories were saved every 2 ps for subsequent analyses.

## ■ ASSOCIATED CONTENT

### Supporting Information

Figure S1: Chromatogram of 1 mg/mL tabersonine extracted from *Voacanga africana* beans. Figure S2: SEC standard calibration curve. Figure S3: Surface plasmon resonance sensorgrams. Table S1: Experimentally measured and theoretical isotopic peaks of tabersonine. This material is available free of charge via the Internet at http://pubs.acs.org/.

## ■ AUTHOR INFORMATION

### Corresponding Authors

*(J.Z.) E-mail: zhengj@uakron.edu.
*(F.Z.) E-mail: fzhou@calstatela.edu.

### Author Contributions

T.K. and L.Z. performed the ThT, AFM, and cytotoxicity experiments. X.W. obtained the CD spectra and SPR data. A.J. and B.Z. conducted SEC. X.Y. and J.Z. carried out the MD simulation, and J.Z. and F.Z. directed the research and wrote the manuscript.

### Funding

This work was supported by the National Institutes of Health (SC1NS070155-01), the National Key Basic Research Program of China (2014CB744502), a 2011 Collaborative and Innovative Grant from Hunan Province of China, and the National Science Foundation (no. 1112105 to F.Z. and nos. CBET-0952624 and CBET115844 to J. Z.). J.Z. thanks the support from Alzheimer Association for a New Investigator Research Grant (2015-NIRG-341372). A.J. acknowledges support from the National Natural Science Foundation of China (no. 81071230) and the China Scholarship Council.

### Notes

The authors declare no competing financial interest.

## ■ ACKNOWLEDGMENTS

We thank Prof. J.-J. Liu for providing the purified tabersonine for this study.



DOI: 10.1021/acschemneuro.5b00015
*ACS Chem. Neurosci.* 2015, 6, 879−888

## ABBREVIATIONS

ThT, thioflavin-T; AFM, atomic force microscopy; SEC, size exclusion chromatography; CD, circular dichroism; SPR, surface plasmon resonance; MTT, 3[4,5-dimethylthiazol-2-yl]-2,5-diphenyl-tetrazolium bromide; AD, Alzheimer's disease; $t_R$, retention time; MD, molecular dynamics

## REFERENCES


(1) Selkoe, D. J. (1991) The molecular pathology of Alzheimer's disease. *Neuron 6*, 487−498.

(2) Hardy, J. A., and Higgins, G. A. (1992) Alzheimer's disease: the amyloid cascade hypothesis. *Science 256*, 184−185.

(3) Hardy, J. (1997) The Alzheimer family of diseases: many etiologies, one pathogenesis? *Proc. Natl. Acad. Sci. U.S.A. 94*, 2095−2097.

(4) Kim, S. H., Vlkolinsky, R., Cairns, N., and Lubec, G. (2000) Decreased levels of complex III core protein 1 and complex V $\beta$ chain in brains from patients with Alzheimer's disease and down syndrome. *Cell. Mol. Life Sci. 57*, 1810−1816.

(5) Yankner, B. A., Duffy, L. K., and Kirschner, D. A. (1990) Neurotrophic and neurotoxic effects of amyloid beta protein: reversal by tachykinin neuropeptides. *Science 250*, 279−282.

(6) Terzi, E., Holzemann, G., and Seelig, J. (1997) Interaction of Alzheimer $\beta$-amyloid peptide(1−40) with lipid membranes. *Biochemistry 36*, 14845−14852.

(7) Bokvist, M., Lindstrom, F., Watts, A., and Grobner, G. (2004) Two types of Alzheimer's $\beta$-amyloid (1−40) peptide membrane interactions: aggregation preventing transmembrane anchoring versus accelerated surface fibril formation. *J. Mol. Biol. 335*, 1039−1049.

(8) Kayed, R., Sokolov, Y., Edmonds, B., McIntire, T. M., Milton, S. C., Hall, J. E., and Glabe, C. G. (2004) Permeabilization of lipid bilayers is a common conformation-dependent activity of soluble amyloid oligomers in protein misfolding diseases. *J. Biol. Chem. 279*, 46363−46366.

(9) Wong, P. T., Schauerte, J. A., Wisser, K. C., Ding, H., Lee, E. L., Steel, D. G., and Gafni, A. (2009) Amyloid-$\beta$ membrane binding and permeabilization are distinct processes influenced separately by membrane charge and fluidity. *J. Mol. Biol. 386*, 81−96.

(10) Simons, M., Schwarzler, F., Lutjohann, D., von Bergmann, K., Beyreuther, K., Dichgans, J., Wormstall, H., Hartmann, T., and Schulz, J. B. (2002) Treatment with simvastatin in normocholesterolemic patients with Alzheimer's disease: A 26-week randomized, placebo-controlled, double-blind trial. *Ann. Neurol. 52*, 346−350.

(11) Zhou, S. X., Zhou, H., Walian, P. J., and Jap, B. K. (2007) Regulation of $\gamma$-secretase activity in Alzheimer's disease. *Biochemistry 46*, 2553−2563.

(12) Kreft, A. F., Martone, R., and Porte, A. (2009) Recent advances in the identification of $\gamma$-secretase inhibitors to clinically test the A$\beta$ oligomer hypothesis of Alzheimer's disease. *J. Med. Chem. 52*, 6169−6188.

(13) Oehlrich, D., Berthelot, D. J. C., and Gijsen, H. J. M. (2011) $\gamma$-Secretase modulators as potential disease modifying anti-Alzheimer's drugs. *J. Med. Chem. 54*, 669−698.

(14) Hawkes, C. A., Ng, V., and Mclaurin, J. (2009) Small molecule inhibitors of A$\beta$-aggregation and neurotoxicity. *Drug Dev. Res. 70*, 111−124.

(15) Wong, H. E., Qi, W., Choi, H. M., Fernandez, E., and Kwon, I. (2011) A safe, blood-brain barrier permeable triphenylmethane dye inhibits amyloid-$\beta$ neurotoxicity by generating nontoxic aggregates. *ACS Chem. Neurosci. 2*, 645−657.

(16) Tjernberg, L. O., Naslund, J., Lindqvist, F., Johansson, J., Karlstrom, A. R., Thyberg, J., Terenius, L., and Nordstedt, C. (1996) Arrest of $\beta$-amyloid fibril formation by a pentapeptide ligand. *J. Biol. Chem. 271*, 8545−8548.

(17) Pallitto, M. M., Ghanta, J., Heinzelman, P., Kiessling, L. L., and Murphy, R. M. (1999) Recognition sequence design for peptidyl modulators of $\beta$-amyloid aggregation and toxicity. *Biochemistry 38*, 3570−3578.

(18) Kim, J. R., and Murphy, R. M. (2004) Mechanism of accelerated assembly of $\beta$-amyloid filaments into fibrils by $KLVFFK_6$. *Biophys. J. 86*, 3194−3203.

(19) Estrada, L. D., and Soto, C. (2006) Inhibition of protein misfolding and aggregation by small rationally-designed peptides. *Curr. Pharm. Des. 12*, 2557−2567.

(20) McLaurin, J., Golomb, R., Jurewicz, A., Antel, J. P., and Fraser, P. E. (2000) Inositol stereoisomers stabilize an oligomeric aggregate of Alzheimer amyloid $\beta$ peptide and inhibit A$\beta$-induced toxicity. *J. Biol. Chem. 275*, 18495−18502.

(21) McLaurin, J., Kierstead, M. E., Brown, M. E., Hawkes, C. A., Lambermon, M. H. L., Phinney, A. L., Darabie, A. A., Cousins, J. E., French, J. E., Lan, M. F., Chen, F., Wong, S. S., Mount, H. T. J., Fraser, P. E., Westaway, D., and George-Hyslop, P. S. (2006) Cyclohexanehexol inhibitors of A$\beta$ aggregation prevent and reverse Alzheimer phenotype in a mouse model. *Nat. Med. 12*, 801−808.

(22) Hong, H. S., Maezawa, I., Yao, N. H., Xu, B. L., Diaz-Avalos, R., Rana, S., Hua, D. H., Cheng, R. H., Lam, K. S., and Jin, L. W. (2007) Combining the rapid MTT formazan exocytosis assay and the MC65 protection assay led to the discovery of carbazole analogs as small molecule inhibitors of A$\beta$ oligomer-induced cytotoxicity. *Brain Res. 1130*, 223−234.

(23) Pokhrel, L., Maezawa, I., Nguyen, T. D. T., Chang, K. O., Jin, L. W., and Hua, D. H. (2012) Inhibition of Acyl-CoA: cholesterol acyltransferase (ACAT), overexpression of cholesterol transporter gene, and protection of amyloid $\beta$ (A$\beta$) oligomers-induced neuronal cell death by tricyclic pyrone molecules. *J. Med. Chem. 55*, 8969−8973.

(24) Hetenyi, C., Szabo, Z., Klement, E., Datki, Z., Kortvelyesi, T., Zarandi, M., and Penke, B. (2002) Pentapeptide amides interfere with the aggregation of $\beta$-amyloid peptide of Alzheimer's disease. *Biochem. Biophys. Res. Commun. 292*, 931−936.

(25) Adessi, C., Frossard, M.-J., Boissard, C., Fraga, S., Bieler, S., Ruckle, T., Vilbois, F., Robinson, S. M., Mutter, M., Banks, W. A., and Soto, C. (2003) Pharmacological profiles of peptide drug candidates for the treatment of Alzheimer's disease. *J. Biol. Chem. 278*, 13905−13911.

(26) Henley, D. B., May, P. C., Dean, R. A., and Siemers, E. R. (2009) Development of semagacestat (LY450139), a functional $\gamma$-secretase inhibitor, for the treatment of Alzheimer's disease. *Expert Opin. Pharmacother. 10*, 1657−1664.

(27) Wood, S. J., MacKenzie, L., Maleeff, B., Hurle, M. R., and Wetzel, R. (1996) Selective inhibition of a fibril formation. *J. Biol. Chem. 271*, 4086−4092.

(28) De Felice, F. G., Houzel, J.-C., Garcia-Abreu, J., Louzada, P. R. F., Jr., Afonso, R. C., Meirelles, M. N. L., Lent, R., Neto, V. M., and Ferreira, S. T. (2001) Inhibition of Alzheimer's disease $\beta$-amyloid aggregation, neurotoxicity, and in vivo deposition by nitrophenols: implications for Alzheimer's therapy. *FASEB J. 15*, 1297−1299.

(29) Yang, F. S., Lim, G. P., Begum, A. N., Ubeda, O. J., Simmons, M. R., Ambegaokar, S. S., Chen, P. P., Kayed, R., Glabe, C. G., Frautschy, S. A., and Cole, G. M. (2005) Curcumin inhibits formation of amyloid $\beta$ oligomers and fibrils, binds plaques, and reduces amyloid in vivo. *J. Biol. Chem. 280*, 5892−5901.

(30) Ma, B. Y., and Nussinov, R. (2002) Stabilities and conformations of Alzheimer's $\beta$-amyloid peptide oligomers ($A\beta_{16-22}$, $A\beta_{16-35}$ and $A\beta_{10-35}$): sequence effects. *Proc. Natl. Acad. Sci. U.S.A. 99*, 14126−14131.

(31) Park, H., and Lee, S. (2003) Determination of the active site protonation state of $\beta$-secretase from molecular dynamics simulation and docking experiment: implications for structure-based inhibitor design. *J. Am. Chem. Soc. 125*, 16416−16422.

(32) Urbanc, B., Cruz, L., Ding, F., Sammond, D., Khare, S., Buldyrev, S., Stanley, H., and Dokholyan, N. (2004) Molecular dynamics simulation of amyloid $\beta$ dimer formation. *Biophys. J. 87*, 2310−2321.

(33) Buchete, N.-V., Tycko, R., and Hummer, G. (2005) Molecular dynamics simulations of Alzheimer's $\beta$-amyloid protofilaments. *J. Mol. Biol. 353*, 804−821.




DOI: 10.1021/acschemneuro.5b00015
*ACS Chem. Neurosci.* 2015, 6, 879−888

(34) Jang, H., Connelly, L., Arce, F. T., Ramachandran, S., Lal, R., Kagan, B. L., and Nussinov, R. (2013) Alzheimer's disease: which type of amyloid-preventing drug agents to employ? *Phys. Chem. Chem. Phys. 15*, 8868−8877.
(35) Tsigelny, I. F., Sharikov, Y., Kouznetsova, V. L., Greenberg, J. P., Wrasidlo, W., Gonzalez, T., Desplats, P., Michael, S. E., Trejo-Morales, M., Overk, C. R., and Masliah, E. (2014) Structural diversity of Alzheimer's disease amyloid-$\beta$ dimers and their role in oligomerization and fibril formation. *J. Alzheimer's Dis. 39*, 583−600.
(36) Lemkul, J. A., and Bevan, D. R. (2010) Destabilizing Alzheimer's $A\beta_{42}$ protofibrils with morin: mechanistic insights from molecular dynamics simulations. *Biochemistry 49*, 3935−3946.
(37) Wang, Q., Yu, X., Patel, K., Hu, R., Chuang, S., Zhang, G., and Zheng, J. (2013) Tanshinones inhibit amyloid aggregation by amyloid-$\beta$ peptide, disaggregate amyloid fibrils, and protect cultured cells. *ACS Chem. Neurosci. 4*, 1004−1015.
(38) Koroch, A. R., Juliani, H. R., Kulakowski, D., Arthur, H., Asante-Dartey, J., and Simon, J. E. (2009) *Voacanga africana*: chemistry, quality and pharmacological activity, in *African Natural Plant Products: New Discoveries and Challenges in Chemistry and Quality*, pp 363−380, American Chemical Society, Washington, DC.
(39) Holland, J. F., Scharlau, C., Gailani, S., Krant, M. J., Olson, K. B., Horton, J., Shnider, B. I., Lynch, J. J., Owens, A., Carbone, P. P., Colsky, J., Grob, D., Miller, S. P., and Hall, T. C. (1973) Vincristine treatment of advanced cancer: a cooperative study of 392 cases. *Cancer Res. 33*, 1258−1264.
(40) Liscombe, D. K., Usera, A. R., and O'Connor, S. E. (2010) Homolog of tocopherol C methyltransferases catalyzes N methylation in anticancer alkaloid biosynthesis. *Proc. Natl. Acad. Sci. U.S.A. 107*, 18793−18798.
(41) Khurana, R., Coleman, C., Ionescu-Zanetti, C., Carter, S. A., Krishna, V., Grover, R. K., Roy, R., and Singh, S. (2005) Mechanism of thioflavin T binding to amyloid fibrils. *J. Struct. Biol. 151*, 229−238.
(42) Ono, K., Condron, M. M., and Teplow, D. B. (2009) Structure−neurotoxicity relationships of amyloid $\beta$-protein oligomers. *Proc. Natl. Acad. Sci. U.S.A. 106*, 14745−14750.
(43) Levine, H. (1993) Thioflavine-T interaction with synthetic Alzheime's disease $\beta$-amyloid peptides: detection of amyloid aggregation in solution. *Protein Sci. 2*, 404−410.
(44) Ono, K., Hasegawa, K., Naiki, H., and Yamada, M. (2004) Curcumin has potent anti-amyloidogenic effects for Alzheimer's $\beta$-amyloid fibrils in vitro. *J. Neurosci. Res. 75*, 742−750.
(45) Feng, Y., Wang, X., Yang, S., Wang, Y., Zhang, X., Du, X., Sun, X., Zhao, M., Huang, L., and Liu, R. (2009) Resveratrol inhibits beta-amyloid oligomeric cytotoxicity but does not prevent oligomer formation. *Neurotoxicology 30*, 986−995.
(46) Tranchida, D., Piccarolo, S., and Deblieck, R. (2006) Some experimental issues of AFM tip blind estimation: the effect of noise and resolution. *Meas. Sci. Technol. 17*, 2630.
(47) Jiang, D., Rauda, I., Han, S., Chen, S., and Zhou, F. (2012) Aggregation pathways of the amyloid $\beta$(1−42) peptide depend on its colloidal stability and ordered $\beta$-sheet stacking. *Langmuir 28*, 12711−12721.
(48) Walsh, D. M., Lomakin, A., Benedek, G. B., Condron, M. M., and Teplow, D. B. (1997) Amyloid $\beta$-protein fibrillogenesis: detection of a protofibrillar intermediate. *J. Biol. Chem. 272*, 22364−22372.
(49) Ahmed, M., Davis, J., Aucoin, D., Sato, T., Ahuja, S., Aimoto, S., Elliott, J. I., Van Nostrand, W. E., and Smith, S. O. (2010) Structural conversion of neurotoxic amyloid-$\beta_{1-42}$ oligomers to fibrils. *Nat. Struct. Mol. Biol. 17*, 561−567.
(50) Amijee, H., Bate, C., Williams, A., Virdee, J., Jeggo, R., Spanswick, D., Scopes, D. I. C., Treherne, J. M., Mazzitelli, S., Chawner, R., Eyers, C. E., and Doig, A. J. (2012) The N-methylated peptide SEN304 powerfully inhibits A$\beta$(1−42) toxicity by perturbing oligomer formation. *Biochemistry 51*, 8338−8352.
(51) Zhang, L., Yagnik, G., Peng, Y., Wang, J., Xu, H., Hao, Y., Liu, Y.-N., and Zhou, F. (2013) Kinetic studies of inhibition of the A$\beta$(1−42) aggregation using a ferrocene-tagged $\beta$-sheet breaker peptide. *Anal. Biochem. 434*, 292−299.
(52) Jan, A., Hartley, D. M., and Lashuel, H. A. (2010) Preparation and characterization of toxic A$\beta$ aggregates for structural and functional studies in Alzheimer's disease research. *Nat. Protoc. 5*, 1186−1209.
(53) Richter, L., Munter, L. M., Ness, J., Hildebrand, P. W., Dasari, M., Unterreitmeier, S., Bulic, B., Beyermann, M., Gust, R., Reif, B., Weggen, S., Langosch, D., and Multhaup, G. (2010) Amyloid beta 42 peptide (A$\beta$42)-lowering compounds directly bind to A$\beta$ and interfere with amyloid precursor protein (APP) transmembrane dimerization. *Proc. Natl. Acad. Sci. U.S.A. 107*, 14597−14602.
(54) Rosenthal, S., and Kaufman, S. (1974) Vincristine neurotoxicity. *Ann. Intern. Med. 80*, 733−737.
(55) Bitan, G., Kirkitadze, M. D., Lomakin, A., Vollers, S. S., Benedek, G. B., and Teplow, D. B. (2003) Amyloid $\beta$-protein (A$\beta$) assembly: A$\beta$40 and A$\beta$42 oligomerize through distinct pathways. *Proc. Natl. Acad. Sci. U.S.A. 100*, 330−335.
(56) Urbanc, B., Cruz, L., Yun, S., Buldyrev, S. V., Bitan, G., Teplow, D. B., and Stanley, H. E. (2004) In silico study of amyloid beta-protein folding and oligomerization. *Proc. Natl. Acad. Sci. U.S.A. 101*, 17345−17350.
(57) Yu, X., Wang, Q. M., Pan, Q. F., Zhou, F. M., and Zheng, J. (2013) Molecular interactions of Alzheimer amyloid-$\beta$ oligomers with neutral and negatively charged lipid bilayers. *Phys. Chem. Chem. Phys. 15*, 8878−8889.
(58) Zheng, J., Jang, H., Ma, B., Tsai, C. J., and Nussinov, R. (2007) Modeling the Alzheimer A$\beta$(17−42) fibril architecture: tight intermolecular sheet-sheet association and intramolecular hydrated cavities. *Biophys. J. 93*, 3046−3057.
(59) Miller, Y., Ma, B., and Nussinov, R. (2010) Polymorphism in Alzheimer A$\beta$ Amyloid organization reflects conformational selection in a rugged energy landscape. *Chem. Rev. 110*, 4820−4838.
(60) Luhrs, T., Ritter, C., Adrian, M., Riek-Loher, D., Bohrmann, B., Dobeli, H., Schubert, D., and Riek, R. (2005) 3D structure of Alzheimer's amyloid-$\beta$(1−42) fibrils. *Proc. Natl. Acad. Sci. U.S.A. 102*, 17342−17347.
(61) Gazit, E. (2002) A possible role for $\pi$-stacking in the self-assembly of amyloid fibrils. *FASEB J. 16*, 77−83.
(62) Tracz, S. M., Abedini, A., Driscoll, M., and Raleigh, D. P. (2004) Role of aromatic interactions in amyloid formation by peptides derived from human amylin. *Biochemistry 43*, 15901−15908.
(63) van der Heijden, R., Jacobs, D. I., Snoeijer, W., Hallared, D., and Verpoorte, R. (2004) The Catharanthus alkaloids: pharmacognosy and biotechnology. *Curr. Med. Chem. 11*, 607−628.
(64) Berhanu, W. M., and Hansmann, U. H. E. (2012) Structure and dynamics of amyloid-$\beta$ segmental polymorphisms. *PLoS One 7*, e41479.
(65) Eisenberg, D., and Jucker, M. (2012) The Amyloid state of proteins in human diseases. *Cell 148*, 1188−1203.
(66) Petkova, A. T., Yau, W. M., and Tycko, R. (2006) Experimental constraints on quaternary structure in Alzheimer's $\beta$-amyloid fibrils. *Biochemistry 45*, 498−512.
(67) Paravastu, A. K., Petkova, A. T., and Tycko, R. (2006) Polymorphic fibril formation by residues 10−40 of the Alzheimer's $\beta$-amyloid peptide. *Biophys. J. 90*, 4618−4629.
(68) Kale, L., Skeel, R., Bhandarkar, M., Brunner, R., Gursoy, A., Krawetz, N., Phillips, J., Shinozaki, A., Varadarajan, K., and Schulten, K. (1999) NAMD2: greater scalability for parallel molecular dynamics. *J. Comput. Phys. 151*, 283−312.
(69) MacKerell, A. D., Bashford, D., Bellott, M., Dunbrack, R. L., Evanseck, J. D., Field, M. J., Fischer, S., Gao, J., Guo, H., Ha, S., Joseph-McCarthy, D., Kuchnir, L., Kuczera, K., Lau, F. T. K., Mattos, C., Michnick, S., Ngo, T., Nguyen, D. T., Prodhom, B., Reiher, W. E., Roux, B., Schlenkrich, M., Smith, J. C., Stote, R., Straub, J., Watanabe, M., Wiorkiewicz-Kuczera, J., Yin, D., and Karplus, M. (1998) All-atom empirical potential for molecular modeling and dynamics studies of proteins. *J. Phys. Chem. B 102*, 3586−3616.


DOI: 10.1021/acschemneuro.5b00015
*ACS Chem. Neurosci.* 2015, 6, 879−888